Environmental Science Nano

ROYAL SOCIETY OF CHEMISTRY

PAPER

View Article Online
View Journal | View Issue

Cite this: *Environ. Sci.: Nano*, 2021, **8**, 1283

Self-indicating and high-capacity mesoporous aerogel-based biosorbent fabricated from cellulose and chitosan *via* co-dissolution and regeneration for removing formaldehyde from indoor air†

Yang Liao and Xuejun Pan *

Received 6th February 2021,
Accepted 29th March 2021

DOI: 10.1039/d1en00122a

rsc.li/es-nano

The present study demonstrated a novel method to fabricate composite aerogels from the two most abundant, natural, and renewable materials on earth (cellulose and chitosan) as a self-indicating biosorbent to remove formaldehyde from indoor air. The aerogel was prepared *via* a process of co-dissolution and regeneration of cellulose and chitosan in an inorganic ionic liquid (a concentrated aqueous solution of lithium bromide), in which cellulose contributes to the porous structure and the physical strength of the aerogel, and chitosan provides the reactive sites (amino groups) to chemically bind formaldehyde. The cellulose–chitosan composite aerogel had a highly porous structure and a large surface area (245 $m^2\ g^{-1}$), which are favorable properties for a sorbent. The results indicated that a composite aerogel (chitosan to cellulose mass ratio 1 : 2) could quickly and irreversibly adsorb formaldehyde with an observed adsorption capacity of up to 7.5 mmol g^{-1} (224 mg g^{-1}) when exposed to excessive formaldehyde. The high adsorption capacity of the composite aerogel was primarily attributed to the chemical adsorption *via* the instantaneous chemical reaction between the amino groups of chitosan and formaldehyde. The physical adsorption of formaldehyde on the aerogel had an insignificant contribution to the overall adsorption capacity. The incorporation of ninhydrin into the composite aerogel provided a real-time color change mechanism to indicate the saturation or expiration of the cellulose–chitosan biosorbent for remediating formaldehyde from indoor air.

Environmental significance

This study demonstrated the fabrication and application of a functionalized mesoporous composite aerogel as a sorbent for removing formaldehyde from indoor air. Formaldehyde is a common indoor air pollutant (a carcinogen), especially in newly built or furnished houses and offices. The mesoporous composite aerogel was fabricated using a co-dissolution and regeneration process from low-cost, abundant, and sustainable cellulose and chitosan. The composite sorbent could remove formaldehyde rapidly and irreversibly (chemically) from the air with a much higher adsorption capacity than the ones previously reported because of its mesoporous structure, large surface area, and more importantly, the presence of the functional group (NH_2). A color-changing mechanism was incorporated for self-indicating the expiration/saturation of the sorbent.

1. Introduction

Formaldehyde is a common harmful indoor air pollutant, especially in newly built or furnished houses and offices. An important source of indoor formaldehyde is the formaldehyde-based resins that are commonly used as adhesives in fiberboards, plywood, particleboard, and other wood products, which are widely employed in home construction as building materials and as components of mobiles and home furnishings, furniture, and cabinets.[1] Also, formaldehyde can be released from smoking and a fireplace.[2] It is known that formaldehyde could irritate the conjunctiva and upper and lower respiratory tract. Symptoms may range from burning or tingling sensations in the eyes, nose, and throat to chest tightness and wheezing, depending upon the level and length of exposure.[3] In 1987, formaldehyde was classified by the U.S. EPA as a probable

Department of Biological Systems Engineering, University of Wisconsin-Madison, 460 Henry Mall, Madison, WI 53706, USA. E-mail: xpan@wisc.edu

† Electronic supplementary information (ESI) available: The experiment setup for formaldehyde adsorption; reaction mechanism of 2,4-DNPH as formaldehyde capture chemical; nitrogen adsorption–desorption isotherm of cellulose–chitosan composite aerogel; mechanism of amino group reacting with formaldehyde; long-term (42 h) formaldehyde removal test by aerogel; reaction mechanism of ninhydrin with an amine to form colored compounds. See DOI: 10.1039/d1en00122a

human carcinogen. Further study and evaluation of the published data led the WHO International Agency for Research on Cancer (IARC) to reclassify formaldehyde as a known human carcinogen associated with nasal sinus cancer and nasopharyngeal cancer. The National Institute for Occupational Safety and Health (NIOSH)'s recommended formaldehyde upper limit for 10 day-average exposure is as low as 0.016 ppm.[4,5]

Many methods have been investigated to remove indoor formaldehyde, such as plant adsorption, physical adsorption, and catalyzed photochemical reactions.[6–14] However, today's means to reduce indoor formaldehyde still heavily rely on traditional passive methods like source control and ventilation improvement. The formaldehyde removal by plants and physical adsorbents is slow, low-capacity, nonspecific to formaldehyde, and even reversible. The catalytic method is expensive and impractical, in particular for residential applications. Therefore, a material that can remove (adsorb) indoor formaldehyde quickly, selectively, and irreversibly with high capacity is eagerly desired, and it would be more desirable if the material could be directly integrated into an air cleaning filter as a sorbent.

Aerogel is a material with extremely low density, high porosity, and high specific surface area.[15] Because of these unique properties, aerogel is an excellent candidate as a sorbent of the materials in the gas phase. For example, amine-functionalized silica-based aerogels were used to remove formaldehyde,[16–18] because amines can react with aldehyde instantaneously *via* nucleophilic addition reaction.

Cellulose and chitosan are the two most abundant natural polymers (polysaccharides) on earth.[19,20] By nature, cellulose (a polymer of D-glucose) is an excellent structural material, and many cellulose-based materials, including aerogels, have been developed using different methods.[21] On the other hand, chitosan (a polymer of D-glucosamine) has one amino group on each glucosamine unit, which can function as a reactive site to adsorb formaldehyde. Therefore, a highly porous cellulose–chitosan composite material, such as aerogel, is expected to be an efficient biosorbent of formaldehyde. Only limited studies were published using chitosan-based materials as formaldehyde sorbents. For example, Nuasaen *et al.*[22] and Yang *et al.*[23] reported that latex particles functionalized with chitosan and chitosan/silver nanocomposites could remove formaldehyde from the air, respectively, but the specific surface area and the formaldehyde adsorption capacity of the materials were not provided. Yang *et al.*[24] developed a chitosan-grafted β-cyclodextrin adsorbent that could uptake formaldehyde up to 15.5 mg g^{-1} in the environment with a formaldehyde concentration of 46.1 mg m^{-3}. The BET specific surface area of the material was only 10.8 m^2 g^{-1}.

Some molten salt hydrates (or inorganic ionic liquids), such as lithium bromide trihydrate (~60 wt% aqueous solution of LiBr), can dissolve polysaccharides such as cellulose and chitosan.[25,26] Using the LiBr system as a solvent, cellulose and whole biomass-based aerogels were successfully fabricated in our previous study.[27] Therefore, the present work aimed to fabricate a mesoporous cellulose–chitosan composite aerogel that has satisfactory physical strength and high adsorption capacity to remove formaldehyde from indoor air. Supposedly, cellulose provides the structural support for the physical strength of the cellulose–chitosan composite aerogel, while chitosan acts as a reactive chemical sorbent of formaldehyde. Besides, the mesoporous structure of the aerogel provides a large surface area to facilitate and enhance both physical and chemical adsorption of formaldehyde. Specifically, cellulose–chitosan composite aerogel was fabricated with lower density and higher specific surface area through a co-dissolution and regeneration process using the LiBr solution as a solvent. The capacity and mechanisms of formaldehyde adsorption by the cellulose–chitosan aerogel were investigated. In addition, a color-change self-indicating mechanism was incorporated into the composite aerogel as a real-time indicator of the service life (expiration) of the biosorbent.

2. Experiment

Materials

Chitosan (medium molecular weight) and cellulose (Avicel PH-101) used in this research were purchased from Sigma-Aldrich (St. Louis, MO). Lithium bromide (99%, anhydrous) was from Alfa Aesar (Ward Hill, MA). Ethanol (200 proof) and *tert*-butanol were purchased from Fisher Scientific (Waltham, MA). Paraformaldehyde was from Electron Microscopy Sciences (Hatfield, PA). 2,4-Dinitrophenylhydrazine (DNPH) from Sigma-Aldrich was used as a formaldehyde trapping chemical,[28] which was impregnated in Sep-Pak C18 cartridges (Waters, Milford, MA). Formaldehyde-2,4-DNPH from Supelco (Bellefonte, PA) was used as a standard in high-performance liquid chromatography (HPLC). HPLC grade acetonitrile was purchased from BDH Chemicals (Radnor, PA). Ninhydrin (puriss. p.a.) was from Fluka Analytical (Honeywell, Mexico City, Mexico).

HPLC analyses

Acetic acid was quantitated using HPLC on an ICS 3000 system (Dionex, Sunnyvale, CA) equipped with a Supelcogel C-610H column (7.8 × 300 mm) and a UV detector at 210 nm. An isocratic flow of 0.1% phosphoric acid was used as the mobile phase at 0.6 mL min^{-1}.[28] Formaldehyde-2,4-DNPH (FA-DNPH) was analyzed on the same HPLC system but with a ZORBAX Rx C8 column (4.6 × 250 mm) at 30 °C, using water/acetonitrile mix (70 : 30, % v/v) as eluent at a flow rate 1.0 mL min^{-1} with a UV-Vis detector at 360 nm.[29]

Aerogel preparation

The process for preparing the cellulose–chitosan composite aerogel is shown in Fig. 1. With fixed 1% (w/w to LiBr solution) cellulose loading, different mass ratios of chitosan to cellulose (1 : 4, 3 : 8, 1 : 2, 5 : 8, 3 : 4, and 1 : 1) were tested. In

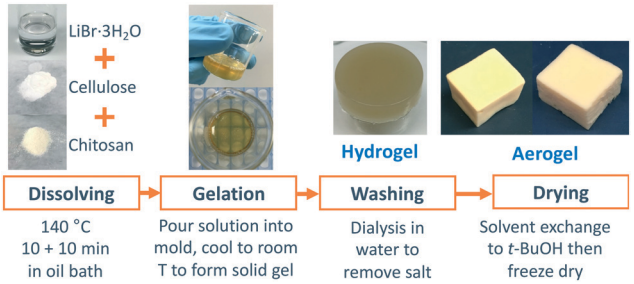

Fig. 1 Schematic process of preparing cellulose–chitosan composite aerogel using the LiBr system.

other words, the combined chitosan and cellulose loadings were 1.25, 1.375, 1.5, 1.625, 1.75, 1.875, and 2% (w/w) in the LiBr solution, respectively.

In brief, weighted chitosan was added into 10 g 60% (w/w) LiBr aqueous solution in a glass vial. The mixture was magnetically stirred at 600 rpm and heated in oil both at 140 °C for 10 min to solubilize chitosan. Then 1% (w/w, to LiBr solution) cellulose was added into the vial, and the mixture was stirred and heated for another 10 min to solubilize the cellulose. The resultant transparent yellowish solution was poured into a beaker and homogenized with a supersonic homogenizer (Sonic 300, Artek, Manassas, Virginia) for 2 min to remove bubbles. When the hot solution was air-cooled to room temperature, a gel was formed. The gel was immersed in a large quantity of deionized water to wash off LiBr through dialysis until no LiBr was detected by $AgNO_3$. Then a gradient solvent exchange process of water–ethanol–*tert*-butanol was conducted to replace the water in the hydrogel with *tert*-butanol. Finally, freeze-drying the gel yielded the cellulose–chitosan composite aerogel. For comparison, pure cellulose aerogels were prepared following a similar procedure with 1, 1.5, and 2% w/w cellulose loading, respectively.

Aerogel characterization

Density was calculated from the mass and volume of the aerogels. Brunauer–Emmett–Teller (BET) total surface area was determined by nitrogen adsorption using a Gemini VII automatic system (Micromeritics, Norcross, GA). Monolith aerogel samples were first degassed at 110 °C overnight (VacPrep 061, Micromeritics, Norcross, GA) and then underwent the nitrogen adsorption–desorption analysis at −196 °C. The BET surface area was calculated using Gemini VII software from the obtained isotherms.

FT-IR spectra of the aerogels were recorded on a Perkin Elmer 100 FT-IR spectrometer (Perkin Elmer, Waltham, MA). All samples were carefully dried before the analysis to avoid the effect of absorbed moisture. The assignments of the FT-IR bands of chitosan were based on the previous studies (Table S1 in ESI†).

The degree of deacetylation of chitosan and the acetyl group in the aerogel was determined by the method published by Zamani *et al.*[30] In short, the chitosan or aerogel sample was treated in sulfuric acid. During the process, the acetyl groups were cleaved as acetic acid, which was quantitated using HPLC, as described above.

The total nitrogen in the aerogel was determined by the micro Kjeldahl method. In brief, the nitrogen in the aerogel was turned into ammonium in concentrated sulfuric acid. Then the ammonium was released as ammonia and captured by boric acid. The nitrogen was quantitated by titration using bromocresol green and methyl red as a mixed indicator.

The morphological structure of the aerogels was observed and recorded on an LEO 1530 (Leo Co., Oberkochen, Germany) scanning electronic microscope (SEM) equipped with a Schottky-type field-emission electron source. The electron gun voltage was 3 kV. Samples were fractured to expose the inner section for observation. Gold coating was applied before SEM imaging.

The mechanical analysis was conducted using an RSA III dynamic mechanical analyzer (TA Instruments, New Castle, DE). Dynamic strain sweep test at room temperature was performed in the compression mode on 8 mm parallel plates, at a frequency of 10 Hz. To fit the testing parallel plates, the aerogels were shaped into cylinders of 8 mm (diameter) × 5 mm (thickness) using a 2 mL microcentrifuge tube as a mold.

Formaldehyde adsorption by the aerogel

The adsorption experiments were conducted in a glass chamber using paraformaldehyde (PFA) as formaldehyde (FA) source, as illustrated in Fig. 2. The cylindrical glass chamber (volume, 2.34 L) has one inlet and one outlet at the bottom, and another outlet at the top. A round flask is connected to the bottom inlet *via* a gas valve to introduce formaldehyde to the chamber. The outlet on the top is used for aerogel loading and gas sampling from the chamber. The system is connected and sealed tightly using glass and silicone tubes

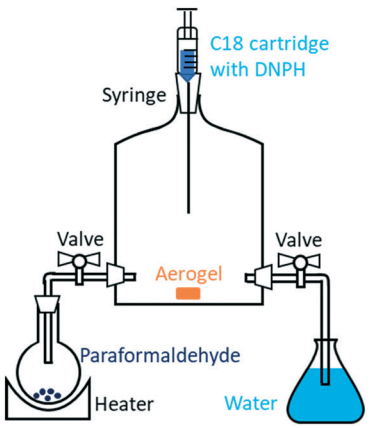

Fig. 2 Illustration of the experimental setup for formaldehyde adsorption by the aerogel.

and stoppers. The stability and leaking of the experiment setup in Fig. 2 were tested, and the result and discussion are shown in Fig. S1 in ESI.†

The adsorption experiment was conducted at room temperature to simulate a real indoor condition. In brief, weighed paraformaldehyde was added into the round flask preheated to 190 °C on an asbestos net heater for gasification. Open the inlet valve and outlet valve at the bottom for 1 hour to allow formaldehyde gas into the main glass chamber. After that, close the valves and wait for 2 h to achieve an equilibrium of the homogeneous distribution of formaldehyde in the chamber. Then quickly but gently open the stopper on the top and add 0.03 g of the aerogel into that chamber. A gas sample of 20 mL was withdrawn at different time points (15, 30, 45, 60, 90, and 120 min, respectively) from the chamber using a syringe equipped with a 15 cm steel sampler through a C18 cartridge impregnated with 0.8 mL trapping solution (130 mg DNPH in 0.5 mL 85% phosphoric acid and 49.5 mL acetonitrile). The formaldehyde capture mechanism is shown in Fig. S2 in ESI.† Then the cartridge was washed with 3 mL acetonitrile. The FA–DNPH in the eluted liquid was analyzed by HPLC, as described above. The formaldehyde concentration in the chamber at time t was calculated from the corresponding concentration of the FA–DNPH derivative. Formaldehyde removal percent at time t is defined as below:

$$R_t = \frac{C_i - C_t}{C_i} \times 100\% \quad (1)$$

where R_t is the formaldehyde removal percentage at time t; C_i is the initial formaldehyde concentration (ppm), and; C_t is formaldehyde concentration (ppm) at time t. Triplicate experiments were run for each sample, and the average result and standard derivation were reported.

Incorporation of ninhydrin as an expiration indicator

After the solvent exchange to replace water with *t*-butanol during the gel fabrication, as described above, the gel was soaked in 0.5% ninhydrin solution in *t*-butanol for 3 hours to disperse ninhydrin into the network of the gel. Then the ninhydrin containing gel was freeze-dried following the same process above.

3. Results and discussion

3.1. Fabrication and characterization of cellulose–chitosan composite aerogels

The mechanism of cellulose dissolution, gelation, and regeneration in the LiBr hydrate system was investigated in our previous studies.[27,31,32] In short, the solubilization of cellulose in the LiBr solution originated mainly from the disruption of the cellulose intermolecular hydrogen bonds *via* the interaction of the hydrated Li^+ with the hydroxyl oxygen of cellulose. After dissolution, cellulose chains were homogeneously dispersed and unentangled in the solution. Upon cooling the solution, the cellulose chains were physically crosslinked by Li^+ *via* coordination, leading to a soft gel with a fixed shape. When the LiBr trapped in the gel was washed out by the water, cellulose regenerated and aggregated to a 3D homogeneous interconnected network of a fibrous skeleton, which was the backbone structure of the resultant hydrogel and aerogel.

It is known that chitosan is soluble in an acidic aqueous system. However, it was found chitosan could be dissolved in the LiBr system without an acid. Therefore, cellulose and chitosan can be co-dissolved in the LiBr system, which makes it easy and feasible to fabricate the cellulose–chitosan composite aerogel *via* the dissolution and regeneration procedure described above. After full dissolution, the solution of cellulose and chitosan in the LiBr system was transparent in a light yellow, as shown in Fig. 1.

Because the amino groups on chitosan are the reactive sites to bind formaldehyde chemically, an aerogel of pure chitosan would supposedly have the highest capacity of adsorbing formaldehyde. However, the attempts to fabricate pure chitosan aerogel failed. The dissolved chitosan in the LiBr solution was a sticky and viscous liquid and did not form an elastic gel after cooling as cellulose did. After washing and drying, the resultant pure chitosan "aerogel" was extremely weak, brittle, and fragile. As discussed in our previous work,[27] because the coordination between a Li^+ ion and an amino group is weaker than that between a Li^+ and a hydroxyl group of cellulose, chitosan chains cannot be crosslinked by Li^+ ions to form a stable and strong network, as cellulose chains can.

Hence, cellulose as a structural material was essential to form the porous structure of the aerogel with sufficient mechanical strength. As shown in Fig. 1, when cellulose was blended with chitosan, an elastic hydrogel with a fixed shape was fabricated successfully. The hydrogel was homogeneous and transparent, indicating that both cellulose and chitosan were completely dissolved and homogeneously mixed and dispersed in the hydrogel. After water washing, the hydrogel became cloudy due to the regeneration (precipitation) of cellulose and chitosan. After the freeze-drying, the obtained aerogel had a homogeneous surface and cross-section. As shown in Fig. 1, the cellulose–chitosan dissolution, hydrogel, and aerogel all had a light-yellow color. The color was probably attributed to the interaction between amino groups of chitosan and a small number of carbonyl groups from cellulose[33] and the chelation effect between amino groups and metal ions (*e.g.*, Li^+ in this case).[34] The color could be also from the degradation products of chitosan under heating conditions.[35]

The FT-IR spectra of cellulose–chitosan composite aerogel and pure cellulose aerogel are shown in Fig. 3. For pure cellulose aerogel, the small peak between 1630–1640 cm^{-1} is caused by the absorbed moisture from the air. The composite aerogel is quite different from the pure cellulose aerogel in the range of 1400–1700 cm^{-1}. The peak at 1655 cm^{-1} is due

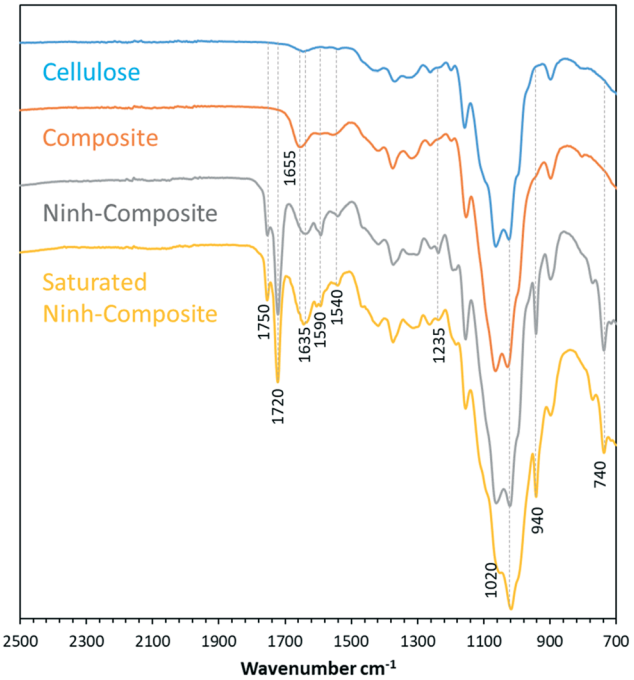

Fig. 3 FTIR spectra of pure cellulose aerogel, cellulose–chitosan (2 : 1 mass ratio) composite aerogel, freshly prepared ninhydrin-incorporated cellulose–chitosan composite aerogel (ninh-composite), and formaldehyde saturated ninhydrin-incorporated cellulose–chitosan composite aerogel (saturated ninh-composite).

to the N–H stretching vibration and the oscillation of C=O in the amide group, which is known as amide I peak. The peak at 1540 cm^{-1} is a typical amide II peak of secondary amide. Both peaks confirm the presence of acetylamino groups in the chitosan, indicating the incompletion of the deacetylation. The N–H bending of the amino group around 1600 cm^{-1} is weak, overlapping with the shoulder of the strong amide bonds. In short, the FT-IR spectra confirmed that the prepared composite aerogel retained the active sites (NH_2) of chitosan.

Density and BET specific surface area of the composite aerogels with different chitosan content are shown in Table 1. Those of the pure cellulose aerogels prepared with 1%, 1.5%, and 2% cellulose loading are listed as well for comparison. As shown in Table 1 and Fig. 4A, the density of all the aerogels increased with the total mass loading. However, the density of the pure cellulose aerogel increased linearly with the total mass loading, while that of the cellulose–chitosan composite aerogels increased slowly and nonlinearly with the total mass loading. In the range from 1% to 2% total mass loading, the composite aerogels had a much lower density than the pure cellulose aerogels, in particular at low mass loading. For example, 1% cellulose + 0.25% chitosan (4 : 1) composite aerogel had lower density than 1% cellulose aerogel, even with 25% more total mass loading. The density of 1% cellulose + 0.5% chitosan (2 : 1) composite aerogel was 24.5 mg cm^{-3}, while that of 1.5% pure cellulose aerogel was 37.3 mg cm^{-3}. With the increased chitosan loading, the density of the composite aerogel started rising quickly and eventually surpassed that of the pure cellulose aerogel at 2% total loading. These observations suggested that a small amount of chitosan could prevent the cellulose-based framework from shrinking during the fabrication, in particular during drying, which resulted in the lower density of the composite aerogels.

The BET specific surface area of the aerogels was investigated (Fig. 4B). The BET specific area of the pure cellulose aerogels (around 210 $m^2\ g^{-1}$) decreased slightly with the cellulose loading from 1 to 2%. However, at a fixed cellulose loading (1%), the specific surface area of the composite aerogels increased first with the chitosan loading, reached a maximum at 0.5% chitosan loading, and then started decreasing with further increased chitosan loading. The specific surface area of the 1 : 1 composite aerogel became smaller than that of the pure cellulose aerogel at the same 2% total mass loading. These results further confirmed that the addition of a small amount of chitosan prevented or reduced the shrinkage of the aerogel during fabrication (drying), and thereby resulting in a more porous structure with a larger specific surface area. The adsorption isotherm of 1.5% cellulose–chitosan (2 : 1) composite aerogel is given in Fig. S3 in ESI,† showing a typical mesoporous material pattern.

The effect of adding chitosan on the density and specific surface area of the composite aerogels can be attributed to the changes to the morphological structure of the aerogels. During the formation of the aerogel network structure due to the regeneration of cellulose and chitosan, hydrogen bonding between cellulose and/or chitosan chains played a very important role. Nitrogen and oxygen have different electronegativity, and therefore the hydrogen bonds they form have different strengths. Freedman studied the

Table 1 Density and BET specific surface area of cellulose–chitosan composite and pure cellulose aerogels at different mass loadings

	Comp 1.25%	Comp 1.375%	Comp 1.5%	Comp 1.625%	Comp 1.75%	Comp 1.875%	Comp 2%	Cell 1%	Cell 1.5%	Cell 2%
Cell to chi ratio	4 : 1	8 : 3	2 : 1	8 : 5	4 : 3	8 : 7	1 : 1	NA	NA	NA
Density (mg cm^{-3})	21.1	23.2	24.5	27.1	29.8	36.4	50.1	21.7	37.3	48.4
BET surface area ($m^2\ g^{-1}$)	231	235	245	241	237	226	198	211	208	209

Note: comp stands for composite aerogel. Cell and chi stand for cellulose and chitosan, respectively. For composite aerogel, cellulose loading was fixed at 1% (w/w, based on LiBr solution), while chitosan loading varied from 0.25% to 1%. The total mass loading for composite aerogel was from 1.25% to 2%, in comparison with pure cellulose aerogel with 1%, 1.5%, and 2% mass loading.

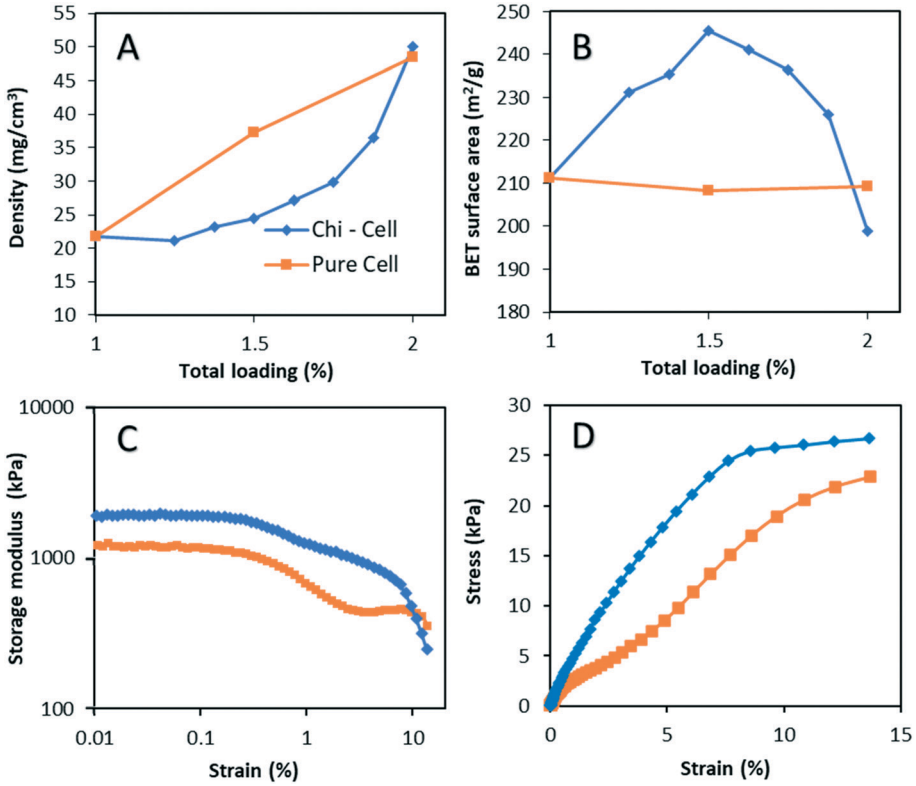

Fig. 4 Comparison of density (A) and BET specific surface area (B) between composite aerogels with different cellulose–chitosan ratios and pure cellulose aerogels; comparison of storage modulus changes (C) and force-strain chart (D) of cellulose–chitosan (2 : 1) composite aerogel and pure cellulose aerogel.

hydrogen bonds of several model compounds and found that the hydrogen bond between hydroxyl and nitrogen was stronger than that between hydroxyls.[36] Murakami and Fujishiro reported that the hydrogen bond with an amino group was one of the strongest hydrogen bonds that a hydroxyl group could form, which was more than twice stronger than those formed with ether, ketone, and nitrile.[37] Yui *et al.* also observed a very strong intermolecular hydroxyl–nitrogen hydrogen bond between chitin chains along the α-axis, resulting in a stable chain stacking.[38] The nitrogen in the amino group is less electronegative than the oxygen in the hydroxyl group. When forming a hydrogen bond, nitrogen tends to donate electron pair and acts as an H bond acceptor, while the oxygen in the hydroxyl group is opposite and tends to be an H bond donor. Therefore, the most favorable hydrogen bond (with higher bonding energy) is O–H···N, which is most likely formed between the cellulose chain and the chitosan chain in the composite. In other words, the hydrogen bonds between chitosan and cellulose should be stronger than those between cellulose chains or chitosan chains. As a result, during the regeneration of cellulose and chitosan, cellulose chains were adhered or bundled together by chitosan chains, which resulted in a thicker, stiffer, and stronger fibrous skeleton and consequently led to the better structural stability of the network to avoid or reduce the shrinkage during washing and drying of the aerogel. This was probably the reason why the composite aerogels at low chitosan loading had lower density and higher specific area than the pure cellulose aerogels. It was observed in our previous research that the cellulose–chitosan composite hydrogel was mechanically stronger than the pure cellulose hydrogel in the rheological test.[39] However, when too much chitosan (larger than 50% in the aerogel) was added, the formation of extensive and strong hydrogen bonds would cause severe shrinkage, thus leading to significantly higher density and lower BET specific surface area.

The mechanical properties of the composite aerogel were investigated *via* dynamic strain-sweep tests shown in Fig. 4C and D. The aerogels deformed under stress but did not fracture or crack even at large strain due to the homogeneous interconnection structure. The 1.5% pure cellulose aerogel had a storage modulus of about 1200 kPa and a yielding pattern with a plateau region.[40] The 2 : 1 composite aerogel had a higher storage modulus (~1900 kPa) and a steeper slope in the strain-force chart in the elastic region, indicating a stronger and stiffer aerogel framework compared to the pure cellulose aerogel. Also, the composite aerogel did not show the plateau region after yielding, probably because of its lower density and more porous structure. These results supported the hypothesis that chitosan reinforces the composite aerogel.

The SEM images of the aerogels support the observation and discussion above. The images of the pure

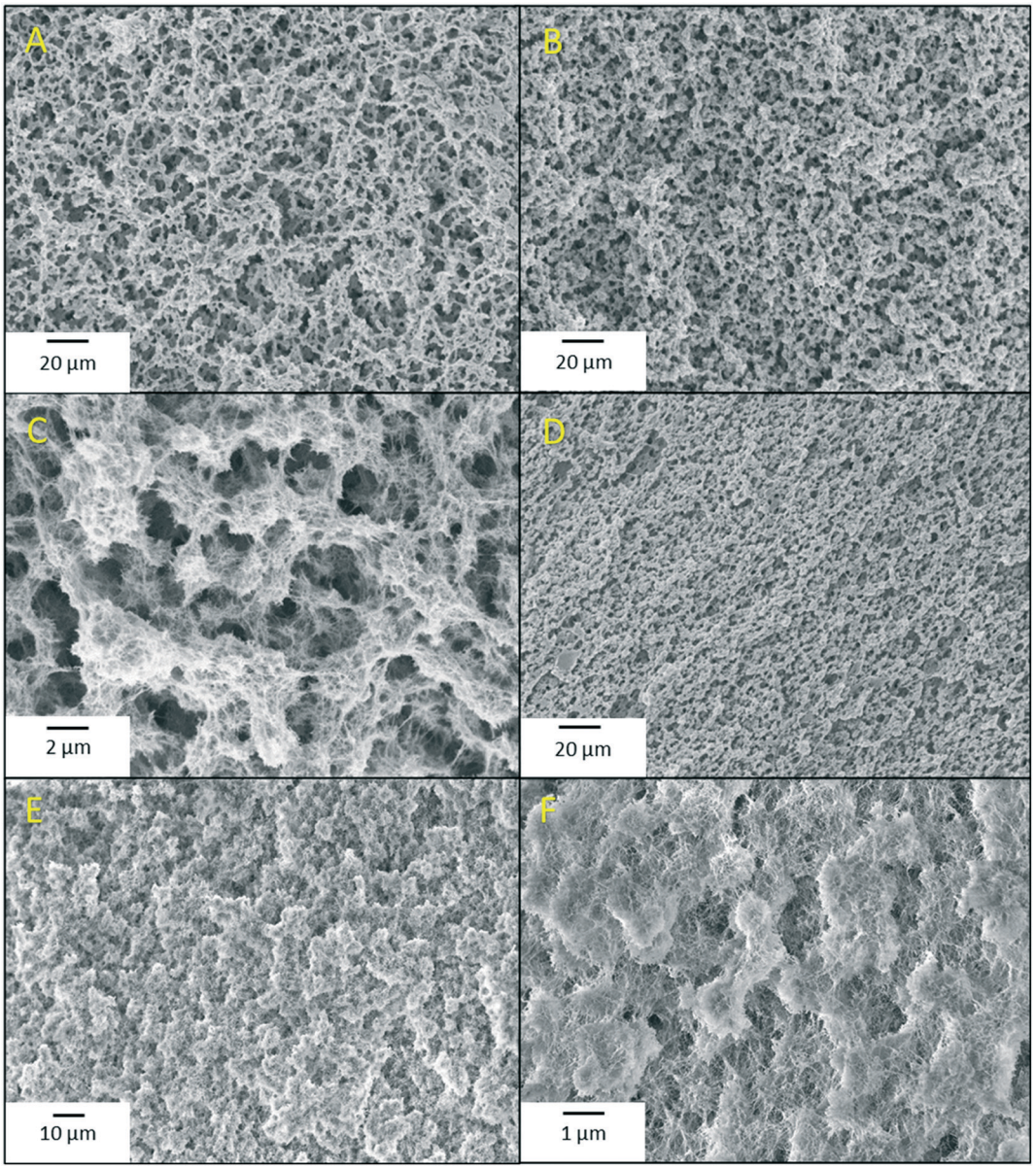

Fig. 5 SEM images of aerogel. A: Pure cellulose aerogel at 1.5% mass loading (w/w, based on LiBr solution); B: composite aerogel with 2 : 1 cellulose–chitosan ratio at 1.5% total mass loading; C: an enlarged image of B showing structure detail; D: composite aerogel with 1 : 1 cellulose–chitosan ratio at 2% total mass loading; E & F: ninhydrin incorporated composite aerogel with 2 : 1 cellulose–chitosan ratio at 1.5% total mass loading saturated with excessive formaldehyde.

cellulose aerogel and the 2 : 1 cellulose–chitosan composite aerogel at the same 1.5% total mass loading are shown in Fig. 5A and B, respectively. The composite aerogel had a thicker framework than the pure cellulose aerogel. When zoomed in (Fig. 5C), it is clear that the framework was structured by the thick bundles of many microfibers, which leads to the highly porous structure and large surface area. Fig. 5D is the image of the 1 : 1 cellulose–chitosan composite aerogel at 2% total mass loading. Compared with that of the 2 : 1 composite aerogel at 1.5% mass loading (Fig. 5B), more chitosan and high total mass load made the aerogel denser, more compact, and less porous.

3.2. Formaldehyde adsorption by the aerogels

As shown in Fig. S4 in ESI,† an amino group can react instantaneously and selectively with formaldehyde to form a methylol intermediate, which is then dehydrated into a stable imine product. The FTIR spectrum (Fig. 3) confirmed the presence of methylol and imine structures in the aerogel after exposed to formaldehyde, which indicates that the cellulose–chitosan aerogel had adsorbed formaldehyde chemically. Besides, because of the large number of mesopores in the aerogel[27,39] and the abundant hydroxyl groups on cellulose and chitosan, the reversible physical adsorption of formaldehyde by

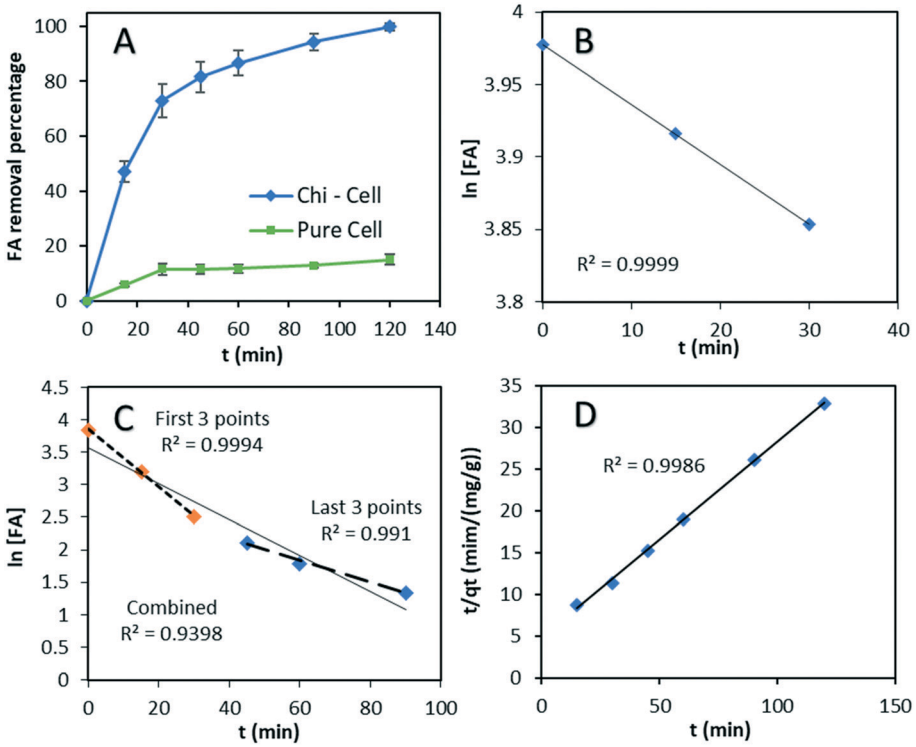

Fig. 6 Formaldehyde adsorption and kinetic study. A: Formaldehyde adsorption profile with time of pure cellulose and cellulose–chitosan (2 : 1 mass ratio) aerogels at an initial formaldehyde concentration of 41.3 mg m^{-3} and room temperature; B: pseudo-first-order plot of pure cellulose aerogel; C: pseudo-first-order plot of cellulose–chitosan (2 : 1 mass ratio) composite aerogel; D: pseudo-second-order plot of the cellulose–chitosan (2 : 1 mass ratio) composite aerogel.

van der Waals force and hydrogen bond would occur as well.[41,42]

The formaldehyde adsorption profile with time by the pure cellulose aerogel is shown in Fig. 6A. Because the cellulose aerogel does not have amino groups, it only physically adsorbs formaldehyde. Once the cellulose aerogel was loaded into the adsorption chamber, the pores on the surface or near the surface quickly adsorbed formaldehyde molecules, leading to a relatively fast initial adsorption rate. After the pores near the surface were saturated, the adsorption rate dropped significantly because the mass transfer of formaldehyde into the deep inside of the aerogel *via* diffusion became the rate-determining factor. For example, about 11.5% of the formaldehyde in the chamber was adsorbed by the cellulose aerogel in the first 30 min. However, extending the adsorption time to 120 min only increased the adsorption to about 15%. The formaldehyde adsorbed at 120 min was 0.48 mg g^{-1}, which was approximately the maximum adsorption capacity of the pure cellulose aerogel because the adsorption curve had reached a plateau (Fig. 6A). Plotting formaldehyde concentration on natural logarithm scale *versus* time in the first 30 min, a linear correlation (R^2 = 0.9999) was obtained (Fig. 6B), confirming that the adsorption of formaldehyde on the pure cellulose aerogel followed the pseudo-first-order in the first 30 min with a reaction rate coefficient k = 0.0041 min^{-1}.

Since the cellulose–chitosan composite aerogel can adsorb formaldehyde both physically and chemically, it adsorbed formaldehyde much more quickly and effectively than the pure cellulose aerogel. As shown in Fig. 6A, a small piece (30 mg) of the composite aerogel (cellulose to chitosan mass ratio, 2 : 1) removed formaldehyde quickly in the chamber by more than 73% in 30 min and almost 100% in 120 min. The formaldehyde adsorbed on the aerogel was 3.22 mg g^{-1}. The theoretical formaldehyde chemical adsorption capacity of the composite aerogel was 52.8 mg g^{-1} (calculated based on the available amino groups in the aerogel). Thus, the cellulose–chitosan composite aerogel used in this test was far from saturation (only ~6% of the theoretical capacity). Comparing the saturated physical adsorption capacity of the pure cellulose aerogel (0.48 mg g^{-1}) and the adsorption capacity of the unsaturated composite aerogel (3.22 mg g^{-1}) under the same conditions, it is clear that the contribution of the physical adsorption was minor to the overall adsorption capacity of the composite aerogel. The chemical adsorption *via* the reaction between amino group of chitosan and formaldehyde shown in Fig. S5† was the dominant adsorption mechanism on the composite aerogel.

The formaldehyde concentration change on the natural logarithm scale *versus* time during the adsorption by the cellulose–chitosan composite aerogel is shown in Fig. 6C. The point at 120 min was excluded because of the extremely low formaldehyde concentration (almost completely adsorbed

on the aerogel). The poor linear-correlation (R^2 = 0.9398) between ln[FA] and t suggested that the formaldehyde adsorption by the composite aerogel do not fit the pseudo-first-order model very well. Dividing the whole adsorption profile into two phases (before and after 30 min), the reaction rate coefficient in the first 30 min was k = 0.0444 min^{-1}, while that in the second phase (30–120 min) was k = 0.0168 min^{-1}. The reaction rate coefficient in the second phase was much lower than that in the first phase but still much higher than that of the pure cellulose aerogel (k = 0.0041 min^{-1}). The high formaldehyde adsorption rate and capacity of the composite aerogel was a result of the synergistic effect of both physical adsorption and chemical adsorption *via* the reaction with the amino group.

The pseudo-second-order model is proposed when chemical reactions control the adsorption kinetics, and therefore it usually fits the adsorption involving chemical reactions better than the pseudo-first-order model. As shown in Fig. 6D, when plotting absorbing time over the formaldehyde absorbed by the aerogel (t/q_t) *versus* time, the pseudo-second-order model indeed fits the adsorption by the composite aerogel much better (R^2 = 0.9986) than the pseudo-first-order model (R^2 = 0.9398). This result is consistent with the previous study.[24]

Extended formaldehyde adsorption for 42 h by the composite aerogel was conducted to investigate the reversibility of the formaldehyde adsorption. As shown in Fig. S5 in ESI,† formaldehyde was completely removed in 2 h and then not desorbed. This indicates that the removal of formaldehyde by the composite aerogel was highly effective and irreversible.

The adsorption experiment above was conducted with an available formaldehyde quantity far below the adsorption capacity of the composite aerogel. In other words, the aerogel was far from being saturated by formaldehyde (only ~6%, as indicated above). To further investigate the adsorption capacity of the composite aerogel, the aerogel was exposed to formaldehyde at an extremely high concentration (~830 mg m^{-3}), which is about 20 times more than that in the previous experiments (~41.3 mg m^{-3}), over an extended time (24 h). It was surprising that the mass of the aerogel increased by 22.4% after the adsorption of formaldehyde. In other words, the formaldehyde adsorbed on the composite aerogel was 7.47 mmol (224 mg) g^{-1}. This was 4 times more than the theoretical chemical adsorption capacity (52.8 mg g^{-1}) of the aerogel, calculated based on the chitosan content in the composite aerogel according to the reaction shown in Fig. S5.† Why the aerogel adsorbed surprisingly more formaldehyde under the extreme conditions is unclear, which needs further investigation. A possibility was that the oligomerization of formaldehyde occurred when adsorbed into the aerogel, which led to the formation and deposition of solid paraformaldehyde and therefore enable the aerogel to uptake much more formaldehyde than the adsorption could. The oligomerization of formaldehyde was kinetically and thermodynamically favorable under the test conditions because the chemical and physical adsorption in the presence of excessive formaldehyde at high concentration created a very high local concentration of formaldehyde on the surface and in the mesopores of the aerogel.[43] It should be noted that the extra high adsorption of formaldehyde was only observed under the extreme condition of excessive formaldehyde at a very high concentration. The aerogel is not expected to adsorb this much formaldehyde from indoor air under normal conditions (at a very low formaldehyde concentration).

The micromorphology of the aerogel changed after the extreme formaldehyde adsorption. As shown in the SEM images, the composite aerogel retained the network structure after the formaldehyde adsorption but became denser and less porous (Fig. 5E and F *vs.* B and C). It is visible in Fig. 5C and F that the pores and the surface of the fibrous skeleton of the aerogel were filled and/or covered by something, which was likely the solid paraformaldehyde formed during the extreme formaldehyde adsorption. As a result, the BET specific surface area of the aerogel dropped from 253 m^2 g^{-1} to 164 m^2 g^{-1} after the adsorption. It should be mentioned that the aerogel sample experienced heating and/or vacuum during the sample preparation and the SEM and BET tests. For example, the aerogel sample was heated overnight at 110 °C under vacuum for degassing before BET test. If the extra amount of formaldehyde adsorbed by the aerogel were in gas form, it would have been removed during the sample preparation or in the SEM and BET experiments. The SEM and BET results provided the indirect evidence of the deposition and presence of solid paraformaldehyde in the aerogel. These results support the hypothesis that the formaldehyde adsorbed by the aerogel under the extreme conditions was oligomerized into solid paraformaldehyde.

The results above suggest that the cellulose–chitosan composite aerogel be an effective sorbent to remove indoor formaldehyde in residences and offices. For example, for a typical 2000 square feet house with 8 feet standard ceiling height, assume that the indoor formaldehyde concentration was 10 times higher than the NIOSH recommended upper limit (0.016 ppm), 1.7 g cellulose–chitosan composite aerogel would be enough to remove all the formaldehyde, based on the theoretical chemical adsorption capacity of 52.8 mg g^{-1} (calculated from the chitosan in the aerogel). Only 0.4 g of the aerogel was needed if using the adsorption capacity observed under the extreme conditions with excessive formaldehyde (224 mg g^{-1}). In practical applications, the composite aerogel biosorbent can be incorporated into, for example, the air filter of a home or office air condition system to remove formaldehyde from the indoor air. The used aerogel could be directly sent to compost because both cellulose and chitosan are biodegradable and have been widely used as a safe ingredient in the food, medical and pharmaceutical industries.[44] Although formaldehyde is a human carcinogen, the resultant chitosan-imine after reacting with chitosan is safe. For example, the chitosan-imine materials crosslinked by formaldehyde and

glutaraldehyde showed biocompatibility in tissue engineering.[45,46]

Isotherm modeling is a common method to investigate the adsorption mechanism. For example, Langmuir model has been widely used for studying the physical adsorption *via* the homogeneous monolayer adsorption, but it is not suitable for the adsorption *via* chemical reactions. For heterogeneous and multi-layer adsorptions, Freundlich model has been proposed. To better understand the adsorption of formaldehyde on the aerogels, the data from the adsorption tests on both the pure cellulose aerogels and the cellulose–chitosan composite aerogels with different initial formaldehyde concentrations were fit into the two models. As shown in Table S2 in ESI,† the physical adsorption of formaldehyde on the pure cellulose aerogel was described well with both models (Langmuir R^2 = 0.9672, and Freundlich R^2 = 0.9674). However, neither model fit the adsorption of formaldehyde on the cellulose–chitosan composite aerogel very well (Langmuir R^2 = 0.8916, Freundlich R^2 = 0.9401) because the chemical adsorption *via* the reaction shown in Fig. S5† was the dominant mechanism of the formaldehyde on the composite aerogel. The Freundlich model fit the adsorption slightly better than the Langmuir model, which is consistent with the heterogeneous and irreversible nature of the formaldehyde adsorption on the composite aerogel. These results suggest that the models for physical adsorptions be inappropriate for studying the chemical adsorption of formaldehyde on the cellulose–chitosan composite aerogel.

3.3. Self-indicating composite aerogel with a real-time indicator of saturation and expiration

When the composite aerogel is used as a sorbent to remove formaldehyde, for example, in a filter or cartridge of a home or office air system, it would be very helpful and convenient to have a real-time indicator of saturation or expiration of the sorbent to inform the user to replace the filter or cartridge. There is a color difference between fresh and saturated composite aerogels, but the difference is too small to distinguish them visually (Fig. 7A). Therefore, an extra indicator is needed.

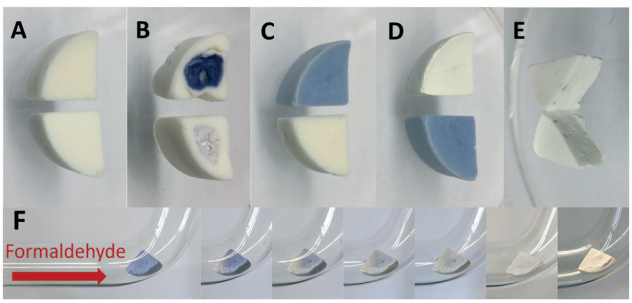

Fig. 7 A, Upper: fresh prepared composite aerogel, lower: saturated aerogel; B, upper: ninhydrin test on composite aerogel, lower: ninhydrin test on cellulose aerogel; C, upper: ninhydrin incorporated composite aerogel, lower: normal composite aerogel cut from the same piece but without ninhydrin; D, upper: formaldehyde saturated ninhydrin incorporated composite aerogel, lower: freshly prepared ninhydrin incorporated composite aerogel; E: cross-section view of formaldehyde saturated ninhydrin incorporated composite aerogel; F: color change of ninhydrin incorporated composite aerogel in formaldehyde gas flow.

Ninhydrin has been used to detect ammonia and primary and secondary amines. When reacting with the amines, a signature dark purple color known as Ruhemann's purple is generated *via* the reactions illustrated in Fig. S6 in ESI.†[47,48] To verify the feasibility of using ninhydrin as an indicator, a drop of 0.5% ninhydrin ethanol solution was applied on the surface of both the cellulose–chitosan composite aerogel and the pure cellulose aerogel. The composite aerogel had a spot in bright purple/blue due to the presence of the NH_2 group, while the cellulose aerogel did not, as shown in Fig. 7B. The observation confirmed that the ninhydrin can detect the availability of the NH_2 group in the composite aerogel. However, this is certainly not a safe and practical way for users to check the expiration of the sorbent at home.

To solve this issue, a method was developed to incorporate ninhydrin into the composite aerogel during fabrication. As described in the experimental section, dissolving ninhydrin in the *t*-butanol for the solvent exchange during the aerogel fabrication, ninhydrin was uniformly dispersed into the aerogel, resulting in a light blue color (Fig. 7C). The hypothesis was that the addition of ninhydrin would turn the composite aerogel in blue, and the color would fade and eventually disappear due to the consumption of the NH_2 group when the aerogel was exposed to formaldehyde, which indicates the saturation or expiration of the aerogel sorbent.

The FTIR spectrum of the composite aerogel with ninhydrin is shown in Fig. 3. The peaks of ninhydrin are visible at 1750, 1720, 1590, 1540, 1235, 940, and 740 cm^{-1}, respectively.[49–51] Besides, there is a peak at 1635 cm^{-1} of C═N in imine formed from the reaction between ninhydrin and chitosan, which is partially overlapped by the chitosan amide I peak. However, the strong and sharp signature peak of Ruhemann's purple at around 1530 to 1580 cm^{-1} (ref. 50 and 51) was not observed in the spectrum, suggesting that the Ruhemann's purple was not formed, as discussed below. The BET specific surface area of the composite aerogel with ninhydrin was 253 $m^2\ g^{-1}$, which was very close to that of the aerogel without ninhydrin, suggesting that ninhydrin did not affect the aerogel structure.

To test whether the ninhydrin-induced blue color fade after the aerogel is saturated by formaldehyde, the aerogel was exposed to a formaldehyde gas flow. As shown in Fig. 7D–F, the color of the aerogel did fade gradually and eventually turned to white. Not only the surface but also the inside of the aerogel turned white (Fig. 7E), indicating that formaldehyde was adsorbed homogeneously across the whole aerogel. These observations confirmed that the ninhydrin-based self-indicating mechanism could indeed indicate the saturation of expiration of the aerogel sorbent to reminding the replacement.

The color-change self-indicating mechanism was further studied. As shown in Fig. S6 in ESI,† once ninhydrin reacts with an amine, a colored intermediate **A** (imine) is formed. The intermediate then undergoes multi-step irreversible reactions to produce the Ruhemann's purple **B** in presence of heat and acid. However, the experimental observations (no signature peak of Ruhemann's purple in FTIR spectrum in Fig. 3 and the blue rather than the purple color of the aerogel in Fig. 7) suggest that the reaction between chitosan and ninhydrin likely stopped at the intermediate **A** rather than ended up to the Ruhemann's purple **B** due to the following reasons. Firstly, the reactions from the intermediate **A** to the Ruhemann's purple **B** are extremely unfavorable when involving C2 of a glucopyranose ring in chitosan because the transformation from sp^3 to sp^2 hybridization is difficult in the glucopyranose ring. Secondly, the conditions of heat and acid required for the reactions were not met during the fabrication of the aerogel. Thirdly, the reaction leading to the Ruhemann's purple **B** shown in Fig. S6 in ESI† is irreversible. In other words, the Ruhemann's purple **B** does not react with formaldehyde to displace ninhydrin. If the Ruhemann's purple **B** was formed during the aerogel fabrication, the purple (blue) color of the aerogel would not fade and vanish when exposed to formaldehyde, which was opposite to the experimental observation above.

The chemical adsorption of formaldehyde on the ninhydrin-containing composite aerogel was investigated using FTIR. When the aerogel was exposed to formaldehyde, the NH_2 groups of the aerogel reacted with formaldehyde, while the ninhydrin in the aerogel remained unchanged. Taking the ninhydrin peaks as a reference, it can be seen that the C═N peak at 1635 cm^{-1} increased substantially in the FTIR spectrum of the formaldehyde-saturated aerogel (Fig. 3), indicating the formation of the imine from the reaction between the amino group of chitosan and formaldehyde (Fig. S4 in ESI†). Besides, the absorbance at 1020 cm^{-1} increased significantly, which is assigned to the C–N bond of the unique carbinolamine intermediate (Fig. S4 in ESI†) formed between formaldehyde and chitosan.[19] Both observations confirmed the occurrence of the reaction between the NH_2 group and formaldehyde.

Based on the observations above, the self-indicating mechanism *via* color change can be summarized as following. When the ninhydrin-containing aerogel (in blue) was exposed to formaldehyde, the free amino groups (not combined with ninhydrin) in the aerogel reacted with formaldehyde first. After the amino groups were completely consumed, the formaldehyde then substituted the ninhydrin from the ninhydrin–chitosan intermediate **A**, which led to the fading and vanishing of the blue color and indicated the saturation (expiration) of the sorbent.

4. Conclusion

This study demonstrated a new method to prepare a composite aerogel as formaldehyde biosorbent from cellulose and chitosan *via* a co-dissolution and regeneration process using lithium bromide molten salt hydrate system as a solvent. The composite aerogel had a mesoporous structure and a large specific surface area. Compared to the pure cellulose aerogel, the cellulose–chitosan composite aerogel had an extremely higher capacity to adsorb formaldehyde. The results confirmed that the chemical adsorption *via* the reaction between amino group of chitosan and formaldehyde was the dominant mechanism of the composite aerogel to uptake formaldehyde. The incorporation of ninhydrin into the aerogel provided a real-time color-change mechanism to indicate the saturation (expiration) of the formaldehyde sorbent. The cellulose–chitosan aerogel has the potential as a marketable biosorbent to remove indoor formaldehyde in residences and offices.

Author contributions

Yang Liao: conceptualization, methodology, formal analysis, investigation, and writing – original drafting, reviewing, and editing; Xuejun Pan: conceptualization, formal analysis, supervision, project administration, writing – reviewing and editing, and funding acquisition.

Conflicts of interest

There are no conflicts of interest to declare.

Acknowledgements

This work was supported by the U.S. Department of Agriculture (USDA) National Institute of Food and Agriculture (NIFA) McIntire Stennis project (WIS01996) and University of Wisconsin Advanced Materials Industrial Consortium (AMIC) Seed Program.

References

1 T. Salthammer, S. Mentese and R. Marutzky, Formaldehyde in the indoor environment, *Chem. Rev.*, 2010, **110**, 2536–2572.
2 P. Kaarakka, M. S. Kanarek and J. R. Lawrence, Assessment and control of indoor air pollution resulting from wood burning appliance use, *Environ. Int.*, 1989, **15**, 635–642.
3 J. Kumaraswamy, R. Hirusappa, J. Naidu and R. Raghavendra, A silent killer in the laboratory–Formaldehyde: Review of effects and management, *Int. J. Oral Maxillofac. Pathol.*, 2011, **2**, 13–19.
4 *An Update on Formaldehyde*, U.S. Consumer Product Safety Commission, Washington, DC, 1997.
5 World Health Organization, International Agency for Research on Cancer (IARC), Monographs on the Evaluation of Carcinogenic Risks to Humans, Vol. 88: Formaldehyde, 2-Butoxyethanol and 1-tert-Butoxypropan-2-ol, 2006, https://monographs.iarc.who.int/wp-content/uploads/2018/06/mono88.pdf.
6 Z. Xu, L. Wang and H. Hou, Formaldehyde removal by potted plant-soil systems, *J. Hazard. Mater.*, 2011, **192**, 314–318.

7 A. Aydogan and L. D. Montoya, Formaldehyde removal by common indoor plant species and various growing media, *Atmos. Environ.*, 2011, **45**, 2675–2682.
8 J. P. Bellat, I. Bezverkhyy, G. Weber, S. Royer, R. Averlant, J. M. Giraudon and J. F. Lamonier, Capture of formaldehyde by adsorption on nanoporous materials, *J. Hazard. Mater.*, 2015, **300**, 711–717.
9 D. Z. Zhao, X. S. Li, C. Shi, H. Y. Fan and A. M. Zhu, Low-concentration formaldehyde removal from air using a cycled storage-discharge (CSD) plasma catalytic process, *Chem. Eng. Sci.*, 2011, **66**, 3922–3929.
10 Z. Xu and H. Hou, Formaldehyde removal from air by a biodegradation system, *Bull. Environ. Contam. Toxicol.*, 2010, **85**, 28–31.
11 Z. Jin, L. Wang, Q. Hu, L. Zhang, S. Xu, X. Dong, X. Gao, R. Ma, X. Meng and F. S. Xiao, Hydrophobic zeolite containing Titania particles as wettability-selective catalyst for formaldehyde removal, *ACS Catal.*, 2018, **8**, 5250–5254.
12 J. Wang, J. Li, P. Zhang and G. Zhang, Understanding the "seesaw effect" of interlayered K+ with different structure in manganese oxides for the enhanced formaldehyde oxidation, *Appl. Catal., B*, 2018, **224**, 863–870.
13 Q. Cheng and G. Zhang, Enhanced photocatalytic performance of tungsten-based photocatalysts for degradation of volatile organic compounds: a review, *Tungsten*, 2020, **2**, 240–250.
14 Q. Zhong, Y. Li and G. Zhang, Two-dimensional MXene-based and MXene-derived photocatalysts: recent developments and perspectives, *Chem. Eng. J.*, 2021, **409**, 128099.
15 A. Du, B. Zhou, Z. Zhang and J. A. Shen, Special material or a new state of matter: a review and reconsideration of the aerogel, *Materials*, 2013, **6**, 941–968.
16 S. Srisuda and B. Virote, Adsorption of formaldehyde vapor by amine-functionalized mesoporous silica materials, *J. Environ. Sci.*, 2008, **20**, 379–384.
17 D. I. Kim, J. H. Park, S. D. Kim, J. Y. Lee, J. H. Yim, J. K. Jeon, S. H. Park and Y. K. Park, Comparison of removal ability of indoor formaldehyde over different materials functionalized with various amine groups, *J. Ind. Eng. Chem.*, 2011, **17**, 1–5.
18 A. M. Ewlad-Ahmed, M. A. Morris, S. V. Patwardhan and L. T. Gibson, Removal of formaldehyde from air using functionalized silica supports, *Environ. Sci. Technol.*, 2012, **46**, 13354–13360.
19 D. Klemm, B. Heublein, H. P. Fink and A. Bohn, Cellulose: fascinating biopolymer and sustainable raw material, *Angew. Chem., Int. Ed.*, 2005, **44**, 3358–3393.
20 M. N. R. Kumar, A review of chitin and chitosan applications, *React. Funct. Polym.*, 2000, **46**, 1–27.
21 K. J. De France, T. Hoare and E. D. Cranston, Review of hydrogels and aerogels containing nanocellulose, *Chem. Mater.*, 2017, **29**, 4609–4631.
22 S. Nuasaen, P. Opaprakasit and P. Tangboriboonrat, Hollow latex particles functionalized with chitosan for the removal of formaldehyde from indoor air, *Carbohydr. Polym.*, 2014, **101**, 179–187.
23 K. H. Yang, Y. C. Liu, C. C. Yu and B. C. Chen, Fabrication of chitosan/silver nanocomposites based on electrochemical methods for removing formaldehyde in air, *Mater. Chem. Phys.*, 2011, **126**, 993–997.
24 Z. Yang, H. Miao, Z. Rui and H. Ji, Enhanced formaldehyde removal from air using fully biodegradable chitosan grafted β-Cyclodextrin adsorbent with weak chemical interaction, *Polymer*, 2019, **11**, 276.
25 S. Sen, J. D. Martin and D. S. Argyropoulos, Review of cellulose non-derivatizing solvent interactions with emphasis on activity in inorganic molten salt hydrates, *ACS Sustainable Chem. Eng.*, 2013, **1**, 858–870.
26 Y. J. Yang, J. M. Shin, T. H. Kang, S. Kimura, M. Wada and U. J. Kim, Cellulose dissolution in aqueous lithium bromide solutions, *Cellulose*, 2014, **21**, 1175–1181.
27 Y. Liao, Z. Pang and X. J. Pan, Fabrication and mechanistic study of aerogels directly from whole biomass, *ACS Sustainable Chem. Eng.*, 2019, **7**, 17723–17736.
28 A. Soman, Y. Qiu and Q. C. Li, HPLC-UV method development and validation for the determination of low-level formaldehyde in a drug substance, *J. Chromatogr. Sci.*, 2008, **46**, 461–465.
29 L. Shuai, Q. Yang, J. Y. Zhu, F. C. Lu, P. J. Weimer, J. Ralph and X. J. Pan, Comparative study of SPORL and dilute-acid pretreatments of spruce for cellulosic ethanol production, *Bioresour. Technol.*, 2010, **101**, 3106–3114.
30 A. Zamani, A. Jeihanipour, L. Edebo, C. Niklasson and M. J. Taherzadeh, Determination of glucosamine and N-acetyl glucosamine in fungal cell walls, *J. Agric. Food Chem.*, 2008, **56**, 8314–8318.
31 N. Li, X. J. Pan and J. Alexander, A facile and fast method for quantitating lignin in lignocellulosic biomass using acidic lithium bromide trihydrate (ALBTH), *Green Chem.*, 2016, **18**, 5367–5376.
32 C. G. Yoo, S. T. Zhang and X. J. Pan, Effective conversion of biomass into bromomethylfurfural, furfural, and depolymerized lignin in lithium bromide molten salt hydrate of a biphasic system, *RSC Adv.*, 2017, **7**, 300–308.
33 J. M. Urreaga and M. U. De la Orden, Chemical interactions and yellowing in chitosan-treated cellulose, *Eur. Polym. J.*, 2006, **42**, 2606–2616.
34 C. L. Schauer, M. S. Chen, M. Chatterley, K. Eisemann, E. R. Welsh, R. R. Price, P. E. Schoen and F. S. Ligler, Color changes in chitosan and poly (allyl amine) films upon metal binding, *Thin Solid Films*, 2003, **434**, 250–257.
35 W. Yue, P. Yao, Y. Wei and H. Mo, Synergetic effect of ozone and ultrasonic radiation on degradation of chitosan, *Polym. Degrad. Stab.*, 2008, **93**, 1814–1821.
36 H. H. Freedman, Intramolecular H-bonds. I. A spectroscopic study of the hydrogen bond between hydroxyl and nitrogen, *J. Am. Chem. Soc.*, 1961, **83**, 2900–2905.
37 S. Murakami and R. Fujishiro, The heats of mixing for binary mixtures. III. The intermolecular energy of hydrogen bonding between alcohol and several other polar molecules, *Bull. Chem. Soc. Jpn.*, 1966, **39**, 720–725.

38 T. Yui, N. Taki, J. Sugiyama and S. Hayashi, Exhaustive crystal structure search and crystal modeling of β-chitin, *Int. J. Biol. Macromol.*, 2007, **40**, 336–344.

39 S. C. Yang, Fabrication and application of cellulose-based hydrogels using lithium bromide molten salt hydrate as solvent, *M.S. Thesis*, University of Wisconsin—Madison, Madison, WI, 2017.

40 L. Zhang, Y. Liao, Y. C. Wang, S. Zhang, W. Yang, X. J. Pan and Z. L. Wang, Cellulose II aerogel-based triboelectric nanogenerator, *Adv. Funct. Mater.*, 2020, **30**, 2001763–2001763.

41 Z. Yan, Z. Xu, J. Yu and M. Jaroniec, Highly active mesoporous ferrihydrite supported Pt catalyst for formaldehyde removal at room temperature, *Environ. Sci. Technol.*, 2015, **49**, 6637–6644.

42 Z. Yan, Z. Xu, J. Yu and M. Jaroniec, Effect of microstructure and surface hydroxyls on the catalytic activity of Au/AlOOH for formaldehyde removal at room temperature, *J. Colloid Interface Sci.*, 2017, **501**, 164–174.

43 J. Kua, J. E. Avila, C. G. Lee and W. D. Smith, Mapping the kinetic and thermodynamic landscape of formaldehyde oligomerization under neutral conditions, *J. Phys. Chem. A*, 2013, **117**, 12658–12667.

44 T. Kean and M. Thanou, Biodegradation, biodistribution and toxicity of chitosan, *Adv. Drug Delivery Rev.*, 2010, **62**, 3–11.

45 A. K. Azab, V. Doviner, B. Orkin, J. Kleinstern, M. Srebnik, A. Nissan and A. Rubinstein, Biocompatibility evaluation of crosslinked chitosan hydrogels after subcutaneous and intraperitoneal implantation in the rat, *J. Biomed. Mater. Res.*, 2007, **83**, 414–422.

46 K. Rinki and P. K. Dutta, Chitosan based scaffolds by lyophilization and sc. CO_2 assisted methods for tissue engineering applications, *J. Macromol. Sci., Part A: Pure Appl. Chem.*, 2010, **47**, 429–434.

47 M. Friedman, Applications of the ninhydrin reaction for analysis of amino acids, peptides, and proteins to agricultural and biomedical sciences, *J. Agric. Food Chem.*, 2004, **52**, 385–406.

48 C. B. Bottom, S. S. Hanna and D. J. Siehr, Mechanism of the ninhydrin reaction, *Biochem. Educ.*, 1978, **6**, 4–5.

49 S. E. Stein, J. M. Rukkers and R. L. Brown, *NIST Standard Reference Database 35, NIST Structures and Properties Database and Estimation Program*, National Institute of Standards and Technology, Gaithersburg, MD, 2018.

50 O. Turhan and E. Tezbaşaran, In situ observation of ninhydrin and phenylhydrazine reaction in solution by FTIR, *Spectrochim. Acta, Part A*, 2013, **113**, 297–301.

51 Y. S. Soliman and T. S. Alkhuraiji, Characterization of a new gel based on alanine–ninhydrin for possible use in radiation dosimetry, *J. Radioanal. Nucl. Chem.*, 2017, **314**, 241–250.